

# The New “*p–n* Junction”: Plasmonics Enables Photonic Access to the Nanoworld

Harry A. Atwater, Stefan Maier, Albert Polman, Jennifer A. Dionne, and Luke Sweatlock

## Abstract

Since the development of the light microscope in the 16th century, optical device size and performance have been limited by diffraction. Optoelectronic devices of today are much bigger than the smallest electronic devices for this reason. Achieving control of light–material interactions for photonic device applications at the nanoscale requires structures that guide electromagnetic energy with subwavelength-scale mode confinement. By converting the optical mode into nonradiating surface plasmons, electromagnetic energy can be guided in structures with lateral dimensions of less than 10% of the free-space wavelength. A variety of methods—including electron-beam lithography and self-assembly—have been used to construct both particle and planar plasmon waveguides. Recent experimental studies have confirmed the strongly coupled collective plasmonic modes of metallic nanostructures. In plasmon waveguides consisting of closely spaced silver rods, electromagnetic energy transport over distances of 0.5 μm has been observed. Moreover, numerical simulations suggest the possibility of multi-centimeter plasmon propagation in thin metallic stripes. Thus, there appears to be no fundamental scaling limit to the size and density of photonic devices, and ongoing work is aimed at identifying important device performance criteria in the subwavelength size regime. Ultimately, it may be possible to design an entire class of subwavelength-scale optoelectronic components (waveguides, sources, detectors, modulators) that could form the building blocks of an optical device technology—a technology scalable to molecular dimensions, with potential imaging, spectroscopy, and interconnection applications in computing, communications, and chemical/biological detection.

**Keywords:** dispersion, nanoparticles, surface plasmons, waveguides.

The invention of the transistor at Bell Laboratories in 1947 has had a transformative effect on technology that is hard to overstate. Born as a discrete device, the transistor's true power and technology leverage came from the integration of first a few, then thousands and now finally millions and billions of transistors in a single monolithic system—at a pace that is elegantly summarized by Moore's law. Photonics has also experienced a Moore's law-like growth in

the bandwidth for information transmission, but not in integration density or component count, and so photonics has mostly been a discrete device technology. This situation is now changing with the advent of integrated photonics based on planar waveguide technologies using dielectric materials.

In this article, we suggest that plasmonics may be an enabling discipline to finally realize photonics at the *nanoscale*, creating

a new “*p–n* junction” in which optical devices can be scaled to and below the scale of the free-space wavelength. Strategies for developing plasmon waveguides at subwavelength lateral dimensions are already becoming apparent using metals and metallocodielectric composites rather than purely dielectric media. While there is a tradeoff between loss and spatial localization in plasmonic structures, centimeter-scale propagation is possible in plasmon waveguides. Such results suggest the potential to create chip-scale integrated photonics with metallic plasmonic interconnects, as depicted in Figure 1.

Plasmons are longitudinal surface charge density modes that exist at conducting interfaces in response to optical excitation. Plasmonic structures can thus be thought to support light waves that run along metallic surfaces in surface plasmon modes.<sup>1</sup> At visible or near-infrared telecommunications frequencies, light waves that run along metal surfaces can have wavelengths as short as 1 nm. Thus, unlike purely dielectric materials, metals and metallocodielectric materials that support surface plasmons offer the unique ability to localize, extract, and enhance electromagnetic fields at metallocodielectric interfaces and in nanostructures.

The unusual dispersion properties of noble metals (including Ag and Au) near the plasmon resonance enables the excitation of surface and resonant modes in nanostructures that access a very large range of wave vectors over a narrow frequency band. This feature, illustrated in the dispersion relation of Figure 2, constitutes a critical design principle for light localization below the free-space wavelength and opens the path to truly nanophotonic or plasmonic optical devices. Combining quantitative electromagnetic simulation methods and a broad portfolio of established and emerg-

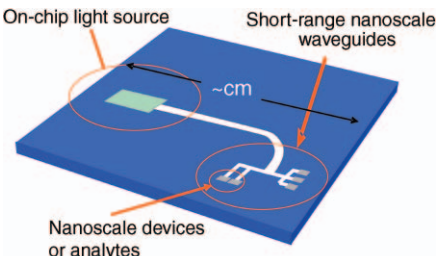
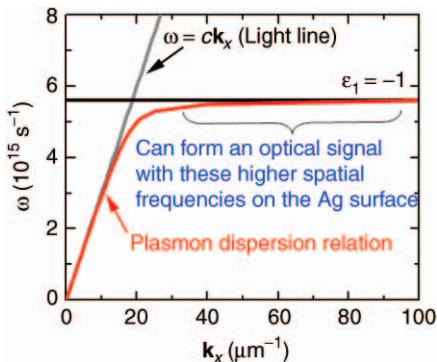


Figure 1. Schematic illustration of a chip-scale plasmonic interconnect network that enables both chip-scale propagation and subwavelength-scale operation. Architectures such as these would transport signals to and from active sources and detectors and efficiently couple into and out of nanometer-scale devices or analytes.



**Figure 2.** A typical planar interface plasmon dispersion relation for a noble metal. Surface plasmons are collective excitations that have nonradiating modes bound to the surface of a metal or thin metallic film. Light can be coupled from free space into the surface plasmon mode only by matching the momentum of the plasmon; this can be done, for example, via prism or grating coupling. Near the plasmon frequency  $\omega_{sp}$ , the real part of the metal dielectric constant  $\epsilon_1$  changes sign from positive to negative, and thus the accessible in-plane wave vectors ( $k_x$ ) can be very large. High wave vectors produce strongly localized optical modes on surfaces, promising potential for imaging and light manipulation at optical frequencies and soft x-ray wavelengths (tens of nanometers).

ing nanofabrication techniques creates the conditions for dramatic scientific progress and a new class of subwavelength optical components.

### Subwavelength-Scale Plasmonic Waveguides

Photonics is in transition toward a world of sub-100-nm designs and components. Advances in particle synthesis and lithography techniques have allowed the fabrication of device components on the nanometer scale. This progress represents an evolution to a subwavelength world, and actual electromagnetic wavelengths in some media—including metals—can be much shorter than free-space optical wavelengths.

Recently, much consideration has been given to using linear metal nanoparticle arrays as waveguides.<sup>2–5</sup> In such arrays, nanoparticles with a diameter much smaller than the wavelength of the exciting light act as electric dipoles.<sup>6–8</sup> Depending on the spacing  $d$  between adjacent nanoparticles, two types of electromagnetic interactions between the particles can be distinguished. For particle spacing

on the order of the exciting wavelength, far-field dipolar interactions with a  $d^{-1}$  dependence dominate.<sup>4,9</sup> However, for particle spacing much smaller than the wavelength of light, near-field dipolar interactions between adjacent particles dominate, with a distance dependence of  $d^{-3}$ . These near-field interactions lead to the formation of collective plasmon modes, in which the individual particles interact strongly and oscillate in phase with one another. The characteristic energies of such collective modes are shifted from that of a single particle and can be observed as a polarization-dependent splitting in the array's absorption spectra.<sup>10–12</sup> In regular one-dimensional chain arrays of metal nanoparticles, this splitting suggests the possibility for waveguiding.

To drive the local dipole sources of these chain arrays, we have investigated optical pulse propagation via full-field finite difference time-domain (FDTD) studies.<sup>13</sup> Figure 3a plots the plasmon pulse position (the location of maximum field amplitude) as a function of time for both longitudinal (squares) and transverse (triangles) excitations. The pulse is launched from a point-dipole source at the start of the chain (a position corresponding to 0 nm on the  $y$  axis), with an energy distribution centered at the resonance energy  $E_0 = 2.4$  eV. Note that this resonance energy corresponds to the  $\mathbf{k} = \pi/2d$  modes with the highest group velocity, allowing for maximal signal propagation. The upper inset of Figure 3a shows a snapshot of the  $x$  component of the electric field in the  $x-y$  plane for longitudinal polarization on a linear color scale. The peak positive (red) and negative (blue) field amplitude positions indicate a wavelength of four times the array period. An analogous snapshot for the  $y$  component of the electric field for transverse polarization is shown in the lower inset of Figure 3a. Linear fits of the datasets in the figure yield values for the group velocities of the transverse and longitudinal modes. These results quantitatively confirm the possibility of using plasmon waveguides for information transport with a group velocity equal to 1% of the speed of light.

The calculations also show the occurrence of negative phase velocities in particle plasmon waveguides when excited in a transverse mode. For the transverse pulse, the group velocity (indicating the direction of energy propagation) and the phase velocity of the individual wave components are antiparallel. This is illustrated in Figure 3b, which shows 10 electric-field snapshots spaced at  $\Delta t = 0.166$  fs apart (10% of a cycle at  $E_0$ ). While the wave packet moves away from the source (the dipole at the left), the individual phase

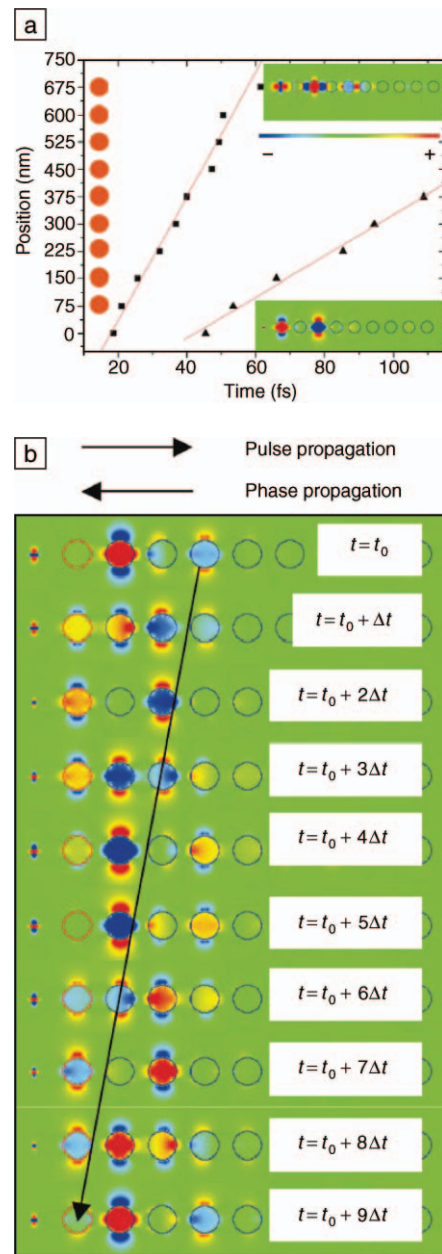


**Figure 3.** (a) Pulse peak positions over time in a plasmon waveguide consisting of spherical particles with a diameter of 50 nm for both longitudinal (solid squares) and transverse (solid triangles) polarization. The solid circles along the ordinate indicate the position of the Au nanoparticles. A snapshot of the  $x$  component of the electric field in the  $x-y$  plane for longitudinal polarization is shown in the upper inset; similarly, a snapshot of the  $y$  component for transverse polarization is shown in the lower inset. (b) Time snapshots of the electric field for transverse pulse propagation show a negative phase velocity with an antiparallel orientation of the phase and group velocities.

fronts are seen to travel toward the source. The diagonal arrow in the figure illustrates this retrograde phase motion for regions of negative amplitude, shown in blue. This behavior arises from a positive group velocity occurring at negative wave vectors (see the transverse-mode dispersion relation of Figure 4, red curve). Nanoparticle chain plasmon waveguides could thus serve as a relatively simple model system for the investigation of negative phase velocity structures.<sup>14,15</sup>

The dispersion relations for Au nanoparticle chain arrays have also been derived from an FDTD analysis. The waveguides were excited with an oscillating point-dipole placed at a distance of 75 nm from the center of the first Au nanoparticle in the waveguide. In consecutive simulations, the point-dipole source was driven continuously at various frequencies in the vicinity of  $E_0$ . The field distribution along the nanoparticle chain structure was then analyzed to determine the wave vector  $\mathbf{k}$  of the propagating waves. Figure 4 shows the dispersion relation for both longitudinal (squares) and transverse (triangles) excitations, as well as the results for the  $\mathbf{k} = 0$  modes obtained by plane wave excitation (circles). The dashed lines indicate the dispersion relation calculated using a simple point-dipole model. The obtained  $\omega(\mathbf{k})$  data are in excellent agreement with the predictions from the point-dipole model, despite the

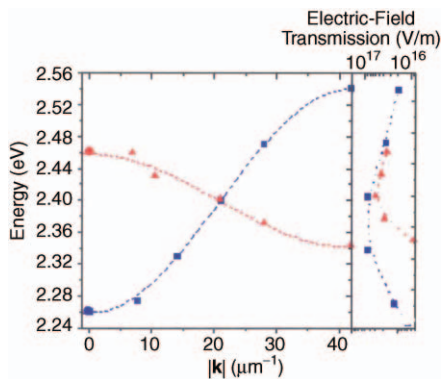


Figure 4. Dispersion relation  $\omega(\mathbf{k})$  for plasmon waveguides consisting of spherical particles for both longitudinal (squares) and transverse (triangles) modes obtained by finite difference time-domain calculations. Also shown are the positions of the  $\mathbf{k} = 0$  modes (circles) obtained from in-phase excitations and the functional dependence predicted by a point-dipole model for the dispersion relation (dashed lines). Right panel: For both longitudinal (squares) and transverse (triangles) modes, the transmitted electric field (top axis) is highest when the first particle is excited at the band center.

limitations of the latter. The right panel of Figure 4 shows the electric-field amplitude at the center of the last nanoparticle for longitudinal excitations (squares). Note that the waveguide loss is at a minimum at the center of the dispersion band, as expected, since the group velocity is at a maximum at this point.

Local excitation and detection of guided light at optical frequencies with a lateral mode profile below the diffraction limit of light provides the most direct evidence for near-field coupling between ordered particles. Indeed, it has been shown both theoretically and experimentally that such arrays, depicted schematically in Figure 5 and experimentally in Figure 6, can guide electromagnetic energy over distances of several hundred nanometers via near-field particle interactions.<sup>16</sup> Highly ordered plasmon waveguides such as those illustrated in Figure 6a can be fabricated by electron-beam lithography and imaged using atomic force microscopy (see Figure 6b) or near-field optical microscopy. Such structures could potentially be used in nanoscale all-optical networks, contributing to a new

class of functional optical devices below the diffraction limit of light.

### Strongly Coupled Plasmon Modes in Nanostructures

Nanoparticle arrays exhibit highly enhanced local fields which can be exploited both for molecular sensors<sup>17–20</sup> and miniature nonlinear optical elements.<sup>21–25</sup> We have recently fabricated closely spaced and contacting linear nanoparticle chains in glass by use of high-energy ion irradiation,<sup>26</sup> as illustrated in Figures 7a and 7b. FDTD simulations indicate dramatic changes in the collective eigenmodes and dispersion properties of the chains when particles are very closely spaced. In the extreme limit of touching particles (see Figures 7c and 7d), two distinct modes are found in the spectrum: one at 0.35 eV (free-space wavelength, 3500 nm) and the other at 1.65 eV (750 nm).

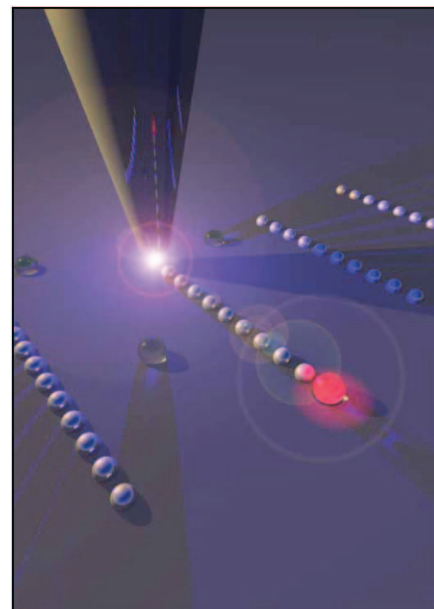


Figure 5. Schematic illustration of local excitation and detection of energy transport in subwavelength-scale plasmon waveguides by near-field optical microscopy. Light emanating from the tip of an illumination-mode near-field scanning optical microscope (NSOM) locally excites a plasmon waveguide. The waveguide transports the electromagnetic energy to a fluorescent polymeric nanoparticle, and the fluorescence intensity for varying tip positions is collected in the far field.

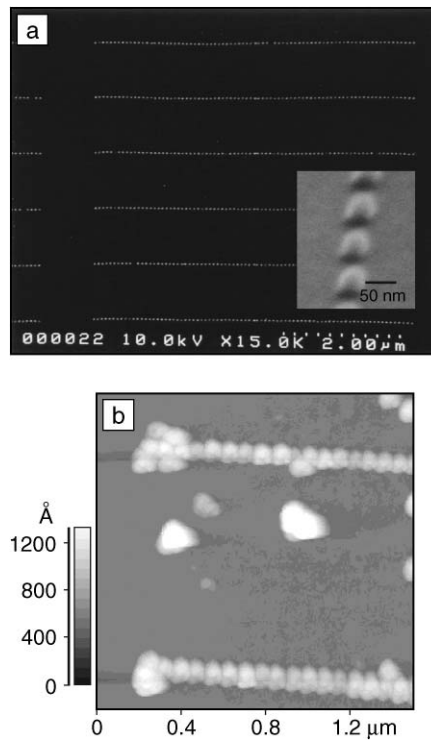
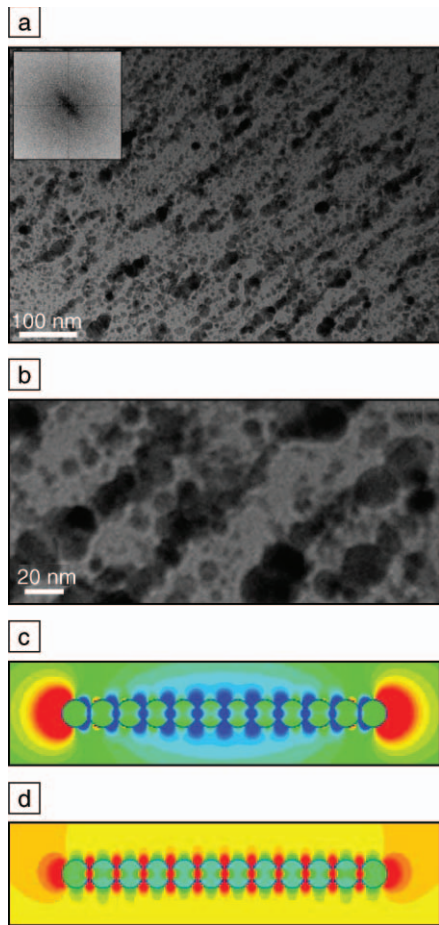


Figure 6. (a) Scanning electron micrograph of plasmon waveguides fabricated by electron-beam lithography, consisting of 50 nm Au particles (see inset) with 75 nm center-to-center spacing. (b) Noncontact atomic force micrograph of Au nanoparticle chain plasmon waveguides with fluorescent polymeric nanospheres positioned at the left end of each plasmon waveguide by scanning force manipulation prior to imaging. The grayscale bar on the y axis indicates the heights of the nanoparticles.

Figures 7c and 7d show the longitudinal component  $E_x$  of the electric field for linear arrays of 12 touching Ag spheres excited at the two resonance frequencies. Red areas



**Figure 7.** (a) Plan-view transmission electron microscopy (TEM) image of Ag nanoparticles in soda lime glass after 30 MeV Si ion irradiation. Alignment of nanoparticles along the ion-beam direction is observed and verified by a spatial fast Fourier transform of the image (inset). (b) TEM indicates a typical particle diameter of 10 nm, albeit with significant size polydispersity, and that the particles are arranged into quasi-linear arrays of up to  $\sim 10$  particles. (c) and (d) Distribution of the  $x$  component of the electric field in the vicinity of an array of 12 Ag particles with 10 nm diameters, illustrating two distinct modes. In (c), an antenna-like mode resembling that of a single elongated wire is excited resonantly at 0.35 eV; in (d) a coupled particle-like mode resembling that of a chain of independent particles is excited resonantly at 1.65 eV. The slight axial asymmetry of the field distribution is caused by superposition of the resonant mode with the exciting plane wave.<sup>36</sup> (Figure taken from Reference 26.)

have positive field amplitude, while blue areas have negative field amplitude. In a snapshot of the chain driven by a longitudinally polarized plane wave at 0.35 eV (Figure 7c), regions of positive  $E_x$  are observed at either end, with negative  $E_x$  throughout the body of the array. This electric-field pattern indicates that positive surface charge is concentrated on the rightmost particle and negative charge on the leftmost particle. The mode is typical of a single-wire antenna and requires surface charge to flow from particle to particle along the entire length of the array.

Alternatively, when the same structure is driven at 1.65 eV (Figure 7d), the coupled-dipole resonance is selectively excited. The field diagram alternates from positive in each dielectric gap to negative inside each particle, as evident from the blue-green color of the particles. This behavior indicates an alternating surface charge distribution in which each individual particle is polarized but electrically neutral. Comparing the field profile of this mode with that of Figure 7c, it is also clear that the coupled dipole resonance exhibits higher energy confinement than the wire-like mode. Thus, in the touching particle configuration, the system can support two kinds of longitudinal resonances: the particles can act as individual coupled dipoles or instead as a single continuous wire antenna.<sup>27</sup>

### Chip-Scale Propagation in Thin-Film Plasmon Waveguides

As early as the 1980s, researchers reported theoretical work on Drude-damping in metals, indicating long-range plasmon propagation at near-infrared wavelengths.<sup>31</sup> However, limitations in fabrication restricted the breadth of optoelectronic applications afforded by thin-film plasmonics. Recent advances in lithography and spectroscopy have allowed us to accurately characterize materials from the mesoscale down. As today's integrated technology develops, it has become both interesting and important to understand the dispersion and attenuation characteristics of surface plasmons on continuous surfaces<sup>32</sup> throughout the electromagnetic spectrum.<sup>33</sup>

Figure 8 illustrates the achievable surface plasmon propagation lengths of thin Ag stripe waveguides embedded in  $\text{SiO}_2$  for both the symmetric ( $L^-$ , Figure 8a) and antisymmetric ( $L^+$ , Figure 8b) electric-field modes,<sup>33</sup> using the complex Ag dielectric constant from Palik's handbook.<sup>34</sup> As the figure shows, for a 12-nm-thick Ag film, propagation is reduced to the micron scale for the symmetric mode (Figure 8a) and increased to tens of centimeters for the antisymmetric mode (Figure 8b) at infrared

frequencies. The inset in Figure 8b also indicates the presence of a local maximum in propagation existing close to the surface plasmon resonance frequency. While not yet experimentally verified, this enhanced propagation at shorter excitation wavelengths could be a promising avenue for future waveguiding research.

The design of integrated photonic circuits requires a delicate balance between mode localization and loss. Unfortunately, the long-range propagation observed in metallic waveguides is accompanied by a large field penetration into the surrounding dielectric. At infrared wavelengths, the long-ranging modes of Figure 8b extend to 5  $\mu\text{m}$  on either side of the Ag waveguide.<sup>33</sup> However, localization can be enhanced by inverting the insulator–metal–insulator waveguiding geometry to one where an insulating core is surrounded by a conducting cladding (a metal–insulator–metal, or MIM, geometry).

The propagating modes of this MIM structure are shown in Figure 9a for  $\text{SiO}_2$  waveguide thicknesses of 12–100 nm.<sup>35</sup> For a 12-nm-thick dielectric waveguide, propagation lengths approach 10  $\mu\text{m}$  at optical frequencies, with distances increasing with  $\text{SiO}_2$  thickness. However, field penetration into the Ag cladding remains approximately constant for all thicknesses (Figure 9b), never exceeding 20 nm. Such results promise potential for integrated plasmonic circuits not unlike the silicon-on-insulator chips of today, with densely packed short-range waveguides couched by layers of long-range waveguides with low confinement factors.

### Conclusions

The potential for surface plasmons to realize both highly localized excitations and long-range waveguiding has been known for more than 30 years. However, their optoelectronic applications have not been realized until recently. No doubt this conversion has been fueled by remarkable progress in nanoscale fabrication and lithography. The past few years have yielded first demonstrations of subwavelength-scale light localization and guiding in plasmonic nanostructures. In metal nanoparticle arrays, propagation distances of over 0.5  $\mu\text{m}$  have been reported, with fields highly confined within the dielectric gaps of these nanostructures. When the gaps are reduced to 1 nm or less, strongly coupled modes are observed with resonance energies that shift substantially from the single-particle resonance energies.

In addition, the properties of thin-film plasmons can now be accurately characterized from realistic models for the complex dielectric function of metals. In Ag films, the surface plasmon exhibits propagation

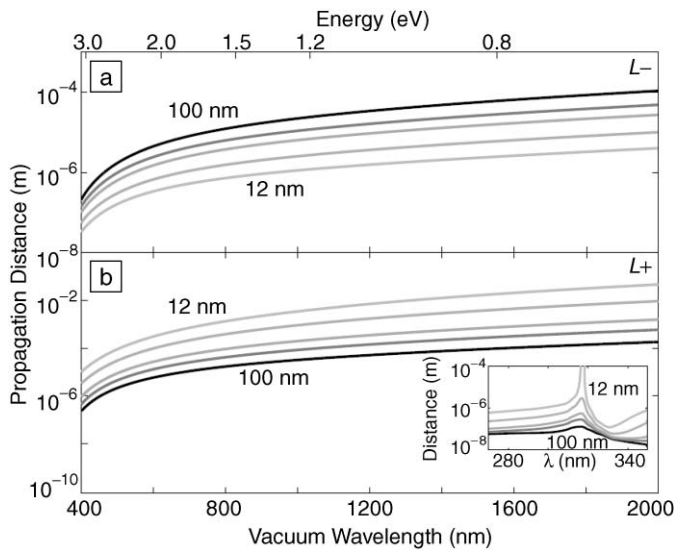


**Figure 8.**  $\text{SiO}_2/\text{Ag}/\text{SiO}_2$  surface plasmon propagation lengths computed with the optical constants from Palik for five different Ag film thicknesses (12 nm, 20 nm, 35 nm, 50 nm, and 100 nm). (a) Lower-energy, symmetric electric-field mode ( $L^-$ ); (b) higher-energy, antisymmetric electric-field mode ( $L^+$ ). The inset in (b) plots propagation distance for wavelengths characteristic of the regime of anomalous Ag dispersion.

lengths exceeding the centimeter scale, with micron-scale field penetration. Using a dielectric core and Ag cladding, mode localization can be further confined to within 20 nm of the waveguide, with propagation lengths exceeding tens of microns.

No doubt plasmonic structures promise a bright future for chip-scale light localization and dispersion engineering. Whether excited in particle or planar arrays, surface plasmons will surely find applications in integrated photonics, contributing a new “*p–n* junction” and ultimately enabling photonic access to the nanoworld.

## References

1. H. Raether, *Surface Plasmons on Smooth and Rough Surfaces and on Gratings* (Springer-Verlag, Berlin, 1988).
2. M. Quinten, A. Leitner, J.R. Krenn, and F.R. Aussenegg, *Opt. Lett.* **23** (1998) p. 1331.
3. M.L. Brongersma, J.W. Hartman, and H.A. Atwater, *Phys. Rev. B* **62** (2000) p. R16356.
4. B. Lamprecht, G. Schider, R.T. Lechner, H. Ditlbacher, J.R. Krenn, A. Leitner, and F.R. Aussenegg, *Phys. Rev. Lett.* **84** (2000) p. 4721.
5. S.A. Maier, M.L. Brongersma, P.G. Kik, S. Meltzer, A.A.G. Requicha, and H.A. Atwater, *Adv. Mater.* **13** (2001) p. 1501.
6. G. Mie, *Ann. Phys.* **25** (1908) p. 377.
7. U. Kreibig and M. Vollmer, *Optical Properties of Metal Clusters* (Springer-Verlag, Berlin, 1994).
8. C. Bohren and D. Huffman, *Absorption and Scattering of Light by Small Particles* (Wiley, New York, 1983).
9. S. Linden, J. Kuhl, and H. Giessen, *Phys. Rev. Lett.* **86** (2001) p. 4688.
10. J.R. Krenn, A. Dereux, J.C. Weeber, E. Bourillot, Y. Lacroute, J.P. Goudonnet, G. Schider, W. Gotschy, A. Leitner, F.R. Aussenegg, and C. Girard, *Phys. Rev. Lett.* **82** (1999) p. 2590.
11. S.A. Maier, M.L. Brongersma, P.G. Kik, and H.A. Atwater, *Phys. Rev. B* **65** 193408 (2002).
12. S.A. Maier, P.G. Kik, and H.A. Atwater, *Appl. Phys. Lett.* **81** (2002) p. 1714.
13. S.A. Maier, P.G. Kik, and H.A. Atwater, *Phys. Rev. B* **67** 205402 (2003).
14. D.R. Smith and N. Kroll, *Phys. Rev. Lett.* **85** (2000) p. 2933.
15. J.B. Pendry, *Phys. Rev. Lett.* **85** (2001) p. 3966.
16. S.A. Maier, P.G. Kik, H.A. Atwater, S. Meltzer, E. Harel, B.E. Koel, and A.A.G. Requicha, *Nature Mater.* **2** (2003) p. 229.
17. F.J. García-Vidal and J.B. Pendry, *Phys. Rev. Lett.* **77** (1996) p. 1163.
18. H. Xu, J. Aizpurua, M. Käll, and P. Apell, *Phys. Rev. E* **62** (2000) p. 4318.
19. A.D. McFarland and R.P. Van Duyne, *Nano Lett.* **3** (2003) p. 1057.
20. D.A. Genov, A.K. Sarychev, V.M. Shalaev, and A. Wei, *Nano Lett.* **4** (2004) p. 153.
21. F. Hache, D. Ricard, and C. Flytzanis, *J. Opt. Soc. Am. B* **3** (1986) p. 1647.
22. Y. Hamanaka, K. Fukata, A. Nakamura, L.M. Liz-Marzán, and P. Mulvaney, *Appl. Phys. Lett.* **84** (2004) p. 4938.
23. R.J. Gehr and R.W. Boyd, *Chem. Mater.* **8** (1996) p. 1807.
24. Y. Shen and P.N. Prasad, *Appl. Phys. B* **74** (2002) p. 641.
25. D. Prot, D.B. Stout, J. Lafait, N. Pinçon, B. Palpant, and S. Debrus, *J. Opt. A* **4** (2002) p. S99.
26. J.J. Penninkhof, A. Polman, L.A. Sweatlock, S.A. Maier, H.A. Atwater, A.M. Vredenberg, and B.J. Kooi, *Appl. Phys. Lett.* **83** (2003) p. 4137.
27. L.A. Sweatlock, S.A. Maier, H.A. Atwater, J.J. Penninkhof, and A. Polman, *Phys. Rev. B* (2004) accepted.
28. K.L. Kliewer and R. Fuchs, *Phys. Rev.* **153** (1967) p. 2.
29. E.N. Economou, *Phys. Rev.* **182** (1969) p. 2.
30. D. Sarid, *Phys. Rev. Lett.* **47** (1981) p. 1927; A.E. Craig, G.A. Oldon, and D. Sarid, *Opt. Lett.* **8** (1983) p. 380.
31. J.J. Burke, G.I. Stegeman, and T. Tamir, *Phys. Rev. B* **33** (1985) p. 8.
32. P. Berini, *Optics Letters* **24** (1999) p. 15; P. Berini, *Phys. Rev. B* **61** (2000) p. 15; P. Berini, *Optics Express* **7** (2000) p. 10; P. Berini, *Phys. Rev. B* **63** (2001) 12.
33. J.A. Dionne, L.A. Sweatlock, H.A. Atwater, and A. Polman, *Phys. Rev. B* (2005) accepted.
34. E. Palik, G. Ghosh, *Handbook of Optical Constants of Solids II* (Academic Press, New York 1991).
35. J.A. Dionne, L.A. Sweatlock, H.A. Atwater, A. Polman (2005) unpublished.
36. Figure adapted from L.A. Sweatlock, S.A. Maier, H.A. Atwater, J.J. Penninkhof et al., “Highly confined electromagnetic fields in arrays of strongly coupled Ag nanoparticles,” *Phys. Rev. B* (2005) accepted. □

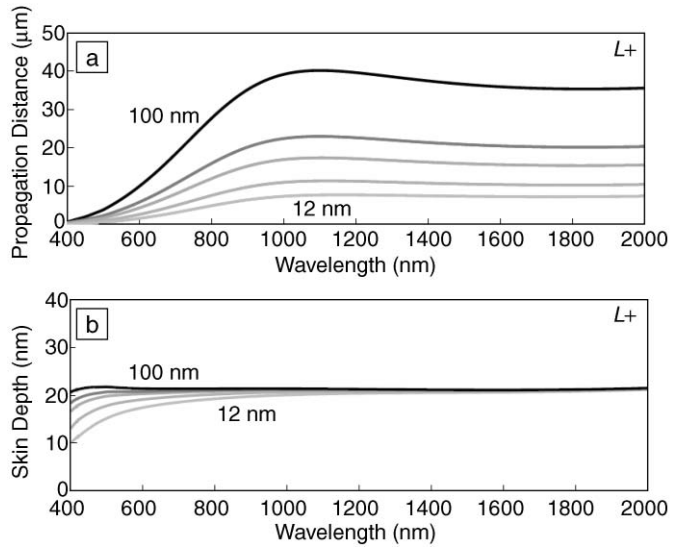


**Figure 9.**  $\text{Ag}/\text{SiO}_2/\text{Ag}$  bound surface plasmon propagation distance (a) and skin depth (b) for  $\text{SiO}_2$  waveguide thicknesses of 12 nm, 20 nm, 35 nm, 50 nm, and 100 nm. While plasmon propagation distances approach tens of microns in the waveguide for a 12-nm-thick film, the mode remains localized within 20 nm of the structure.